Eur. J. Mech. B - Fluids 20 (2001) 727–740

S0997-7546(01)01153-0/FLA

Separation behaviour in front of a two-dimensional fence

Henri A. Siller [a*], Hans-Hermann Fernholz [b]

[a] *DLR Abteilung, Turbulenzforschung Berlin, Charlottenburg, Müller-Breslau-Strasse 8, 10623 Berlin, Germany*
[b] *Hermann-Föttinger-Institut für Strömungsmechanik, TU Berlin, Strasse des 17. Juni 135, 10623 Berlin, Germany*

(Received 6 October 2000; revised 28 February 2001; accepted 8 June 2001)

Abstract – The wall-bounded turbulent shear flow in front of a two-dimensional fence was investigated experimentally. In this prototype of a rapidly separating flow the assumptions for a first-order boundary-layer theory cease to apply. This is caused by the streamline curvature, the ensuing pressure gradient normal to the wall and the large vertical velocity component v in front of the fence. For the present experiment, where the ratio of the boundary layer thickness δ_0 measured without the fence and the fence height h is 0.82, the time mean separation length upstream of the fence l_f is $0.65h$. However, instantaneous reverse flow events can be detected up to 4 mean separation lengths l_f upstream of the fence. The maximum value of the reverse flow factor χ_w is 95% indicating a strong reverse flow region. The experiments were performed by LDA and a wall pulsed-wire skin-friction meter. They show the limits of first-order boundary-layer theory and provide the first comprehensive data set of mean and fluctuating velocities and of wall shear-stress for this type of separating flow. © 2001 Éditions scientifiques et médicales Elsevier SAS

1. Introduction

Step-induced separation occurs both in internal and external flows. In the first case, the flow in a pipe or duct may encounter a sharp-edged ridge or an abrupt contraction and, in the second case, an obstacle be it a spoiler, a fence, or a three-dimensional body. Since such flows have a separation region upstream and downstream of the obstacle, they introduce an 'overwhelming perturbation' in the sense of Bradshaw and Wong [1], meaning that a boundary-layer type flow changes into a free shear-layer type flow. The effects of this perturbation abate only very slowly in downstream direction. Therefore the emphasis of many investigations has been on the development of the second, the downstream, separation region and the redevelopment of the reattached flow, e.g. Castro and Fackrell [2], Durst and Rastogi [3], Dimaczek et al. [4], Schofield and Logan [5], Castro and Epik [6], and Siller [7].

LDA measurements of mean velocity profiles and Reynolds stresses upstream of a two-dimensional rib, however in a fully developed duct flow, were performed by Tropea and Gackstatter [8] and Acharya et al. [9].

The present investigation is concerned with the flow domain upstream of a fence which is a prototype of rapidly separating flows (Bradshaw and Galea [10]) and at the same time an example of a wall-bounded shear flow for which the simplifications leading to the boundary-layer model cease to apply. This is caused by the curvature of the streamlines due to the obstacle, the ensuing pressure gradient normal to the wall and the large velocity component normal to the wall near the fence. Furthermore, it is difficult to define an edge of the boundary layer since the velocity maximum occurs far away from the wall.

Earlier investigations of the separated flow upstream of an obstacle were performed by Head and Rechenberg [11], Fernholz [12], Bradshaw and Galea [10], Good and Joubert [13], Ranga-Raju et al. [14],

* Correspondence and reprints.
E-mail address: Henri.Siller@DLR.de (H.A. Siller).

for example. Their goal has been to check the validity range of Preston tubes in an adverse pressure gradient, to determine the drag as a function of fence height or to validate the separation criterion of Stratford and Townsend (Townsend [15]).

Föttinger [16] visualised the wall-bounded shear layer approaching a vertical plate (see also Batchelor [17], plate 7). Besides the strong curvature of the streamlines in the xy-plane the photograph shows a large corner vortex with its axis in the z-direction below the stagnation line on the vertical wall, together with a chain of smaller vortices extending upstream on the horizontal wall below the separating streamline. In this type of flow, both the reattachment line on the upstream front of the fence and the separation line on the plate upstream of the fence show instantaneous fluctuations although their positions remain steady in the mean.

The boundary layer upstream of a ring-like insert in the entry flow of a circular pipe was investigated by measuring the static pressure and the skin-friction distribution in streamwise direction by Head and Rechenberg [11] and the mean velocity profiles and the circumferential skin-friction distribution by Fernholz [12]. Although the developing turbulent boundary layer in the pipe should have been axisymmetric, it showed variations of the skin-friction of 26% around the circumference increasing to even larger variations with decreasing distance to the ring. Therefore the non-uniform skin-friction distribution (measured by means of a surface fence) displayed a highly three-dimensional behaviour of the separation region. A similar behaviour upstream of obstacles has been detected in several other wind tunnels.

In order to generate a nearly straight separation line over the central 60% of the span of the fence, great care was taken for the present experiment to make the upstream flow uniform. The wind-tunnel nozzle and the plate in the test-section were properly aligned and a perforated metal sheet with square openings was placed a short distance downstream of the woven filter mat at the entrance of the settling chamber. The separation line was checked by oil-flow visualisation and by spanwise skin-friction measurements which then varied only within a range of $\pm 2.5\%$ (measured at $x = 440$ mm without the fence present).

The length l_f of the mean reverse-flow region depends on several parameters, such as the state of the boundary layer, the ratio of the fence height h to the height of the test section H (the blockage), the ratio of spanwise width B to h, the ratio δ_0/h, the Reynolds number $Re_h = (hU_{\mathrm{ref}})/\nu$ and the free-stream turbulence level Tu_δ. Here, δ_0 denotes the thickness of the boundary layer at the position of the obstacle in the absence of the obstacle. Wieghard [18] and Good and Joubert [13] found that the extent of the upstream influence of the obstacle on the boundary layer relative to the fence height h increased with h/δ_0 (see also Lighthill [19] for a laminar boundary layer). Low values of the blockage H/h increased the length of the separation region (Castro and Fackrell [2]) but the blockage effect became negligible for values $H/h \geqslant 9$ (Siller [7]).

The present experimental investigation was part of a larger project with the aim of reducing the length of the separation region downstream of a fence by introducing an oscillating cross flow through a spanwise slot upstream of the fence ([7]). Therefore, the parameters governing the upstream flow field were chosen such that the downstream separation region was reasonably large and independent of the Reynolds number. The parameters used in this experiment were as follows: $H/h = 6.75$; $B/h = 22$; $Re_h = 1.05 \times 10^4$ (based on U_{ref}); $\delta_0/h = 0.82$; free-stream turbulence level $Tu_\delta = 0.3\%$.

In this flow configuration measurements were taken of the velocity field, the Reynolds stresses, the wall pressure, and the skin-friction in order to investigate the development of the adverse-pressure gradient turbulent boundary layer with rapid separation and the breakdown of the boundary-layer concept. The measurements were performed by Laser-Doppler-Anemometry (LDA) and a wall pulsed-wire probe (WPW). The experimental investigation was accompanied by a numerical calculation using large eddy simulation (LES) (Orellano and Wengle [20]).

2. Test rig and measuring techniques

The measurements were performed in the test section of a blower-type wind tunnel (*figure 1*). The test wall was the floor plate made of cast aluminium. It was situated 17 mm above the downstream edge of the wind-tunnel nozzle (with a contraction ratio of 5.3) in order to remove the nozzle boundary-layer. Pressure taps and plugs to house the skin-friction meter were aligned 8 mm away from the centre line of the floor plate. Spanwise distributions of the wall data were also measured by inserting probes into a a narrow strip of PVC flush with the wall which could be traversed in spanwise direction.

One side wall and the roof of the test section consisted of glass plates to allow optical access for the LDA system. In order to generate a uniform flow at the entrance of the test section, the settling chamber was equipped with a non-woven filter mat and a single, precisely manufactured perforated metal plate (64% open area ratio). The radial fan was driven directly by an electric motor of 4.5 KW with electronic speed control.

The upstream laminar boundary layer was tripped by means of a Velcro tape, which was 2.6 mm high and located at $x = 68$ mm downstream of the elliptical nose of the test wall. The fence was mounted at $x_f = 638$ mm and was $h = 20$ mm high. The distance from the position of the transition trip to the position of the fence was $\Delta x_f/h = 28.5$ and may be considered large compared with the ratio $l_f = 0.65\,h$, where $l_f \approx 13$ mm is the distance between the mean separation line, located near $x = 625$ mm, and the fence on the centreline of the test section. The fence had a sharp upper edge with a backward chamfer of 45° and was mounted at $x_f = 638.0$ mm downstream of the leading edge. The overall length of the test section was 1500 mm.

In contrast to many earlier investigations where the measurements were taken with the probes mounted at a fixed x-position and the obstacle moved along the x-axis, for this investigation the fence was fixed and the probes were positioned relative to it. Thus, the length of the flat-plate boundary-layer upstream of the fence and the ratio of boundary-layer thickness to fence height δ_0/h (measured with the fence removed from the test section) were kept constant.

For the measurements of the mean and fluctuating velocities, a two-component fibre-optic LDA system by Dantec powered by a 300 mW argon-ion laser was used. It operated in backscatter mode with two Dantec burst-spectrum analyser (BSA) modules operating in continuous mode. Coincidence checking was performed in private/private mode and frequency shifting was applied in order to discriminate between forward and backward flow. The focal length of the probe was 600 mm and the measuring volume was an ellipsoid of revolution with a length of 1.4 mm and a diameter of 88 µm. The laser optics were inclined by an angle of approximately $\phi = 6°$ towards the horizontal plane in order to allow measurements close to the wall. For measurements of the four profiles closest to the fence, located within 0.75 h upstream of the fence, the laser optics were also rotated by 4.5° around the vertical axis.

Measurement errors were checked by measuring a turbulent boundary-layer profile under identical conditions with the LDA system and a hot-wire anemometer. The differences between the two measurements were within

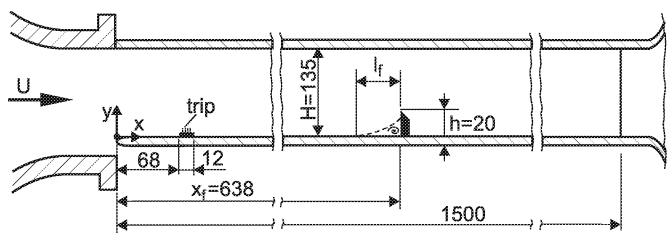

Figure 1. Experimental set-up.

$+2.5\% - 3.5\%$ for the mean value and below 5.0% for the fluctuating component of the velocity except for the region near the wall ($y^+ < 3$), where the hot-wire is known to give erroneous results.

The wall shear-stress τ_w and the reverse-flow factor at the wall χ_w were measured using a wall pulsed-wire (Bradbury and Castro [21] and Castro [22]). χ_w is the ratio of heat pulses detected at the upstream wire, i.e. indicating reverse flow, to the total number of heat pulses at both sensor wires. The wall pulsed-wire probe was set up for high sensitivity, using sensor wires with a diameter of 2.5 μm and an active length of 2.5 mm positioned 0.085 mm above the wall. The sensor wires were 1.4 mm apart in the streamwise direction with the pulser wire in the middle. The pulser wire had a diameter of 5 μm and was 5.0 mm long. The wall pulsed-wire probe was calibrated against a Preston tube in the turbulent boundary layer of the test-section with the fence removed.

3. Experimental results

Figure 2 presents two smoke-wire flow visualisations in the region near the fence. The photographs show two different instances of the same turbulent flow. The bulk velocity and all other parameters were the same as for the measurements. There is turbulent flow near the wall and close to the fence and a turbulent shear layer separating at the tip of the fence. The separation region itself is almost entirely devoid of smoke, because the streak lines that were marked with smoke are deflected by the fence. As the streak lines approach the fence, they converge in the accelerating flow and move up and over the fence.

Figure 3 shows the velocity vector field together with the static pressure field. The static pressure was calculated along the streamlines using Bernoulli's equation under the assumption that the Bernoulli constants remained constant. The Bernoulli constants for each streamline were calculated from the boundary-layer profile $u(y)$ and the static pressure at the wall at the reference position ($(x_f - x)/h = 10.78$; $(x_f - x)/l_f = 16.58$). At this position, streamline curvature is negligible and the pressure is constant across the boundary layer. The static pressure inside the separation regions up- and downstream of the fence could not be calculated because of the closed streamlines.

Figure 3 shows how the static pressure rises in the streamwise direction and normal to the streamlines where they curve concavely as the flow approaches the fence. Above the fence and immediately downstream, the static pressure is reduced due to the contraction of the flow. The velocity vectors in *figure 3* show the large vertical component immediately upstream of the fence.

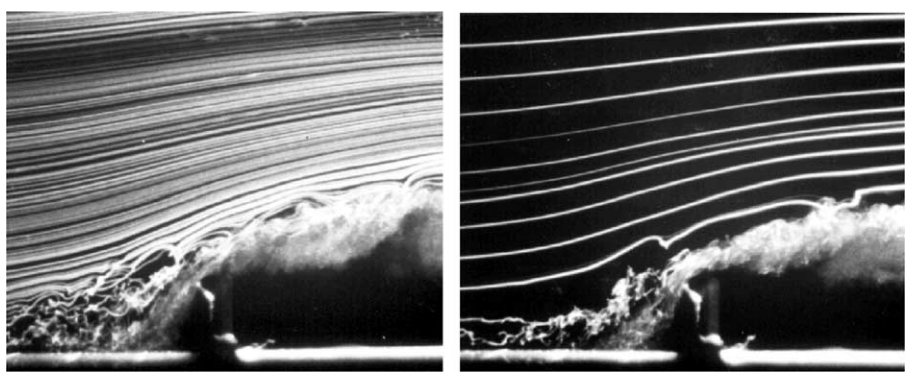

Figure 2. Typical smoke-wire flow visualisations, the mean flow velocity is the same as for the measurements.

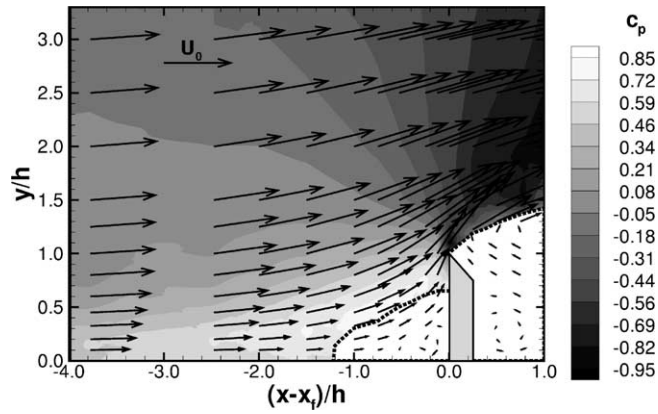

Figure 3. Velocity and static pressure fields upstream of the fence, the static pressure is calculated using Bernoulli's equation; dotted line: separating streamline.

3.1. Static pressure and wall shear-stress

Figure 4 presents characteristic wall data as a function of the dimensionless length $(x_f - x)/l_f$ on a logarithmic scale to enlarge the region near the fence. Also shown is the shape parameter H_{12} that will be discussed below. The fence is fixed at position x_f and x is the distance from the leading edge in streamwise direction. The surface pressure coefficient c_p and the skin-friction coefficient c_f were both made dimensionless by the dynamic pressure at the upstream reference position ($(x_f - x)/h = 10.78$; $(x_f - x)/l_f = 16.58$). The c_p-distribution shows the decrease of the pressure gradient and a plateau, which is indicative of a closed separation bubble, near the region where separation occurs. The first upstream influence of the pressure increase on the wall is detected at $x/h \approx 11$ (compared with a value of 13 taken from the correlation of Good and Joubert [13] which was obtained with lower blockage). At the position where the mean skin-friction changes sign ($c_f = 0$), the reverse-flow factor has a value of 54% which is close enough to 50% found in earlier investigations for the separation point (e.g. Dengel and Fernholz [23], or Alving and Fernholz [24]). The distribution of χ_w shows that instantaneous reverse flow extends upstream four units of the mean reverse-flow length and that the maximum value of χ_w is 95% which is characteristic of a strong reverse-flow region (Fernholz [25]). Additional

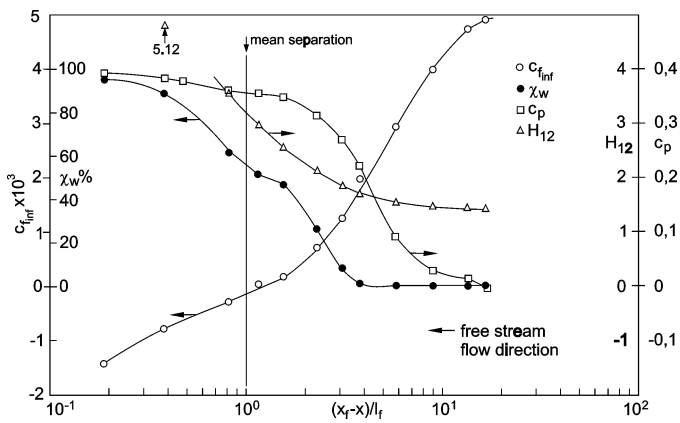

Figure 4. Streamwise distribution of the static pressure coefficient c_p, the skin-friction coefficient $c_{f\,\mathrm{inf}}$, the reverse-flow parameter χ_w, and the shape parameter H_{12} (lines are for visual aid only).

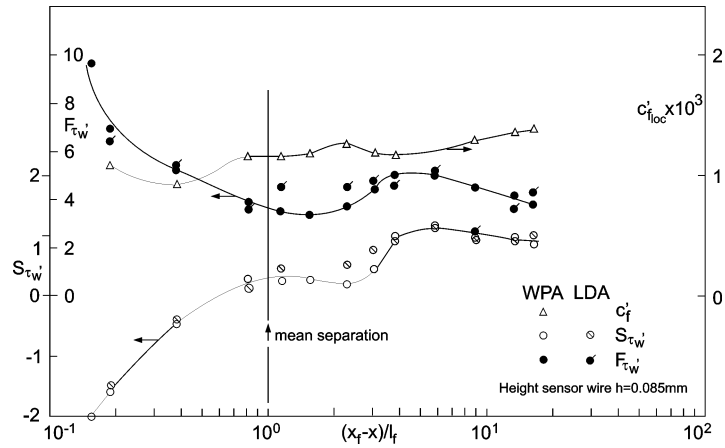

Figure 5. Moments of the fluctuating skin-friction coefficient c'_f, its skewness $S_{\tau'_w}$ and flatness $F_{\tau'_w}$ (lines are for visual aid only).

measurements (not shown here) were taken very close to the fence, where $(x_f - x)/l_f < 0.2$. Because probes could only be mounted at fixed positions in the floor plate, the fence had to be moved relative to the probe. These measurements show a small decrease of χ_w and an increase of c_f at $(x_f - x)/l_f = 0.008$.

Figure 5 presents the streamwise distribution of the coefficient of the fluctuating skin-friction

$$c'_{f\,\mathrm{loc}} = 2\sqrt{\overline{\tau'^2}}/\left(\rho\, u^2_{\overline{u'v'}=0}\right)$$

and its higher moments, the skewness

$$S_{\tau'_w} = \overline{\tau'^3}/\left(\overline{\tau'^2}\right)^{3/2}$$

and the flatness

$$F_{\tau'_w} = \overline{\tau'^4}/\left(\overline{\tau'^2}\right)^2.$$

They were measured by means of a wall pulsed wire at a height $y = 0.085$ mm and by LDA at $y = 0.1$ mm and are actually measurements of the streamwise velocity component.

The coefficient of the fluctuating skin-friction shows a relatively small change in comparison with the distribution shown by Alving and Fernholz [24], decreasing from about 1.4×10^{-3} to 0.9×10^{-3} in the reverse-flow region.

With the onset of instantaneous reverse flow ($\chi_w > 0$), the skewness begins to decrease from its maximum value of about 1 changing sign in the separation region. The sign of the skewness $S_{\tau'_w}$ reaches a value of -2 and, since the skewness is attributed to energetic events (sweeps) bringing higher momentum fluid to the wall, these events are more likely in the reverse-flow direction (Alving and Fernholz [24]).

The flatness factor $F_{\tau'_w}$ decreases from 5 to 3.5 at the onset of instantaneous reverse flow and then increases to values of approximately 10 towards the fence. Such a large $F_{\tau'_w}$ can be attributed to the impingement onto the near-wall fluid of higher-speed fluid transported by the corner vortex.

The spreading of instantaneous reverse flow away from the wall begins at $(x_f - x)/l_f = 3.81$. This process is seen best from the profiles of the reverse-flow factor $\chi(y)$ which reach a value of 50% at $(x_f - x)/l_f = 1.15$ (*figure 6*). The locus $y(\chi = 50\%)/h$ reaches its maximum value of 0.11 at $(x_f - x)/l_f = 0.19$, or in fence heights $(x_f - x)/h = 0.125$, and at the same x-station we find the height of the region of instantaneous reverse

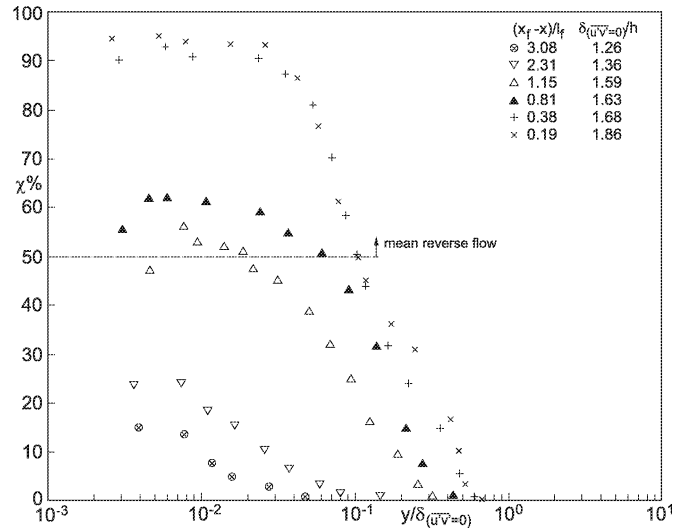

Figure 6. Profiles of the reverse-flow parameter $\chi(y)$ at various streamwise positions x.

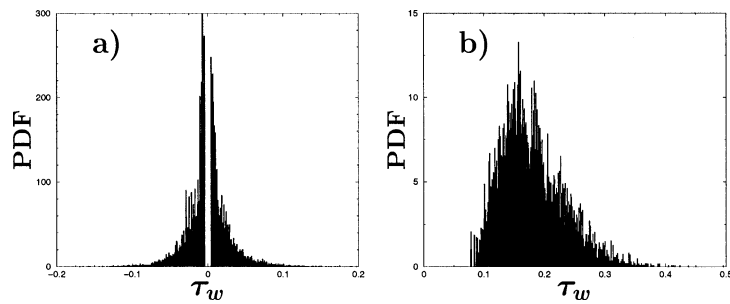

Figure 7. Probability density functions of the fluctuating skin-friction; (a) at $x = 623.0$ mm and (b) at $x = 422.0$ mm.

flow at $y_{\chi=0\%}/h = 0.65$. This value corresponds well with the position of the mean stagnation line on the front face of the fence, between $0.6 \leqslant y/h \leqslant 0.7$, determined from an oil-flow visualisation.

Figure 7 presents the probability-density functions of the wall shear-stress for two different locations, at the reference position $(x_f - x)/l_f = 16.58$, where the boundary layer is not disturbed by the fence yet, and at $(x_f - x)/l_f = 1.15$, close to the time mean separation position. At $(x_f - x)/l_f = 16.58$, the distribution is skewed towards larger values of τ_w because of frequent sweep events that bring energetic fluid close to the wall. The skewness $S_{\tau_w'}$ (see *figure 5*) shows a value of approximately one, the value to be expected in a zero pressure-gradient boundary-layer (Fernholz and Finley [26]). Close to separation, at $(x_f - x)/l_f = 1.15$, the distribution is relatively symmetric, indicating that strong events are almost equally likely to occur in the up- and in the downstream direction. The skewness at this point is $S_{\tau_w'} \approx 0.3$. Because the wall pulsed-wire anemometer rejects samples that exceed a maximum time-of-flight, there is a gap around $\tau_w \approx 0$ in *figure 7(a)*.

3.2. Mean velocity

Figure 8 shows some mean velocity profiles in inner-law scaling. The log law is well confirmed at the upstream reference position ($(x_f - x)/l_f = 16.58$) and begins to become invalid at $(x_f - x)/l_f = 3.81$, where χ_w rises above 1%, a limit found by Dengel and Fernholz [23] earlier.

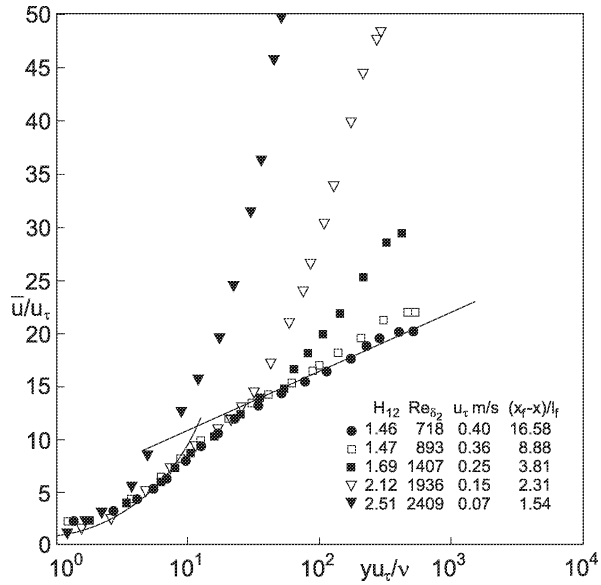

Figure 8. Profiles of the mean velocity in inner-law scaling (log-law constants $\kappa = 0.4$, $C = 5.10$).

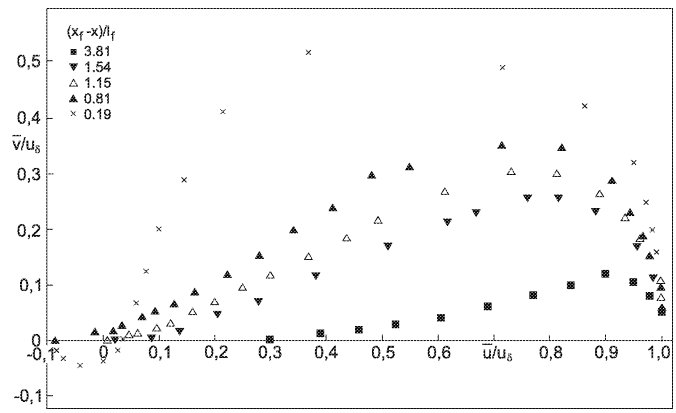

Figure 9. Polar plot of wall-normal and streamwise mean velocity in front of a fence.

Further insight into the flow upstream of the fence can be obtained from the polar diagram $\overline{v}/u_\delta$ against $\overline{u}/u_\delta$ (*figure 9*) where $\overline{v}$ is the mean velocity normal to wall. Since first order boundary-layer theory assumes that in general $\overline{v}/u_\delta$ should be much smaller than $\overline{u}/u_\delta$ this condition is more and more violated the closer the fence is approached. Here we have used u_δ for normalisation which is the maximum value of $\overline{u}$ at a given position along the x-axis.

The behaviour of the velocity components $\overline{u}$ and $\overline{v}$ is, of course, reflected in the distribution of the static pressure $p(y)$ normal to the wall shown in *figure 3*. The pressure and velocity distributions close to the fence raise the question where the validity range of a first order boundary-layer model ends. In order to demonstrate the problem, we have plotted first the development in streamwise direction of the velocity ratio $u_{\delta_{99.5}}/U_{\text{ref}}$ where $u_{\delta_{99.5}}$ is defined as $0.995\,\overline{u}_{\max}$, together with the corresponding dimensionless boundary-layer thickness $\delta_{99.5}/h$. *Figure 10* shows that $u_{\delta_{99.5}}/U_{\text{ref}}$ increases as the fence is approached because the fence contracts the flow. Also, $\delta_{99.5}/h$ increases abruptly between $16.58 < (x_f - x)/l_f < 3.81$ and then slowly decreases as the fence is

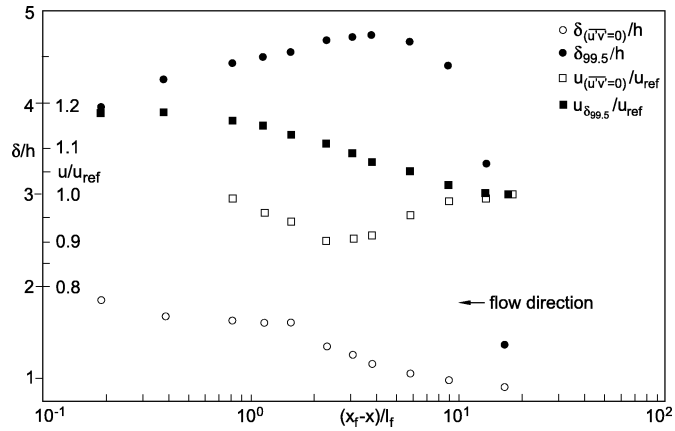

Figure 10. Streamwise distribution of characteristic length scales and mean velocities at the edge of the boundary layer in front of a fence with height h.

approached further. As the flow approaches the fence, the potential flow above the boundary layer is accelerated due to the contraction of the flow. However, the flow within the boundary layer is retarded until the flow separates. In this case, the traditional definition of the boundary-layer edge as the position where the local velocity reaches 99.5% of the free stream velocity ceases to make sense.

We have therefore chosen a different boundary-layer thickness $\delta_{\overline{u'v'}=0}$. This is the location normal to the wall where the Reynolds shear stress $\overline{u'v'}$ approaches zero. Because experimental data is always scattered, the values of $y(\overline{u'v'}=0)$ and $y(u/U_{\text{ref}}=0.995)$ were determined from cubic-spline interpolations of the measured velocity profiles. With this definition of the boundary-layer edge, the decrease of $\overline{u}_{\overline{u'v'}=0}/\overline{u}_{\text{ref}}$ agrees qualitatively with the development of the velocity profiles, and $\delta_{\overline{u'v'}=0}/h$ increases more slowly than $\delta_{99.5}/h$, at least up to $(x_f-x)/l_f=2.31$, This means that for a case of 'rapid separation' in front of an obstacle, first order boundary-layer theory should cease to be valid at about two mean separation lengths upstream of the obstacle. We have integrated the displacement and the momentum-loss thickness, δ_1 and δ_2, up to $\delta_{\overline{u'v'}=0}$ and determined the shape parameter $H_{12}=\delta_1/\delta_2$ the development of which is shown in *figure 4*. At separation, the value of $H_{12}\approx 3.18$ is slightly higher than predicted by Dengel and Fernholz [23] ($H_{12\,\text{sep.}}=2.89\pm 0.10$), but it is still close enough not to invalidate our assumption of the modified boundary-layer thickness.

3.3. Turbulence measurements

We begin by giving a brief survey about the measurements performed. Profiles of the Reynolds stresses are plotted in *figures 12(a)* to *(c)* with the distance y normal to the wall, made dimensionless by $\delta_{(\overline{u'v'}=0)}$, and $\overline{u_i'u_j'}$ by $u^2_{\tau_{\text{ref}}}$ at the reference position $(x_f-x)/l_f=16.58$. The present test arrangement did not allow measurements of the fluctuating velocity component w' in spanwise direction.

Figures 13(a) and *(b)* show the first term of the production terms of the transport equation for the turbulent kinetic energy

$$(\overline{u'v'})\frac{\partial\overline{u}}{\partial y}+\left(\overline{u'^2}-\overline{v'^2}\right)\frac{\partial\overline{u}}{\partial x}$$

and for the Reynolds shear stress

$$\overline{v'^2}\,\frac{\partial\overline{u}}{\partial y}+\overline{u'^2}\,\frac{\partial\overline{v}}{\partial x}.$$

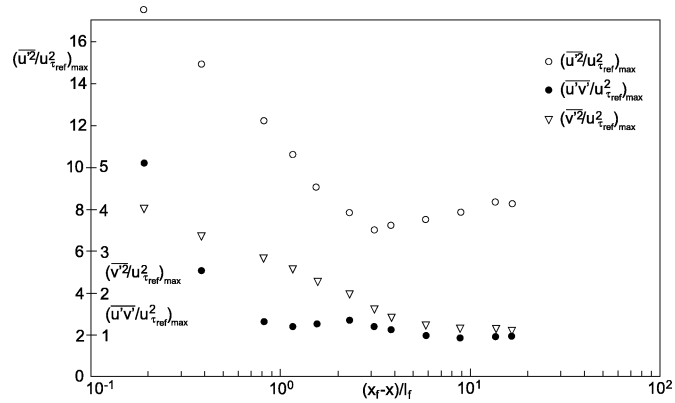

Figure 11. Streamwise development of the maximum values of the Reynolds stresses.

Finally the skewness and flatness are presented in *figure 14*.

An overview about the development of the maximum values of the two Reynolds normal stresses and the Reynolds shear stress in streamwise direction is given in *figure 11* (note the different scales). The normal stresses show a behaviour characteristic of that seen in other adverse pressure-gradient boundary-layers (e.g. Dengel and Fernholz [23]) with a rapid increase near separation with $\overline{u'v'}$ lagging behind.

Since the mean shear $\partial\overline{u}/\partial y$ decreases near the wall and increases away from the wall in an adverse pressure-gradient boundary-layer, this results in a shift of both the production peak and the Reynolds stress peaks to roughly the middle of the boundary layer (*figures 12(a)* to *(c)*), see also Alving and Fernholz [24]. The upstream profiles at the reference position $(x_f - x)/l_f = 16.58$ agree well with the DNS data of Spalart [27] or Khanna [28] which confirms the reliability of the LDA measurements and the quality of the starting values for a numerical simulation. Both $\overline{u'^2}$ and $\overline{u'v'}$ decrease in the inner layer with increasing pressure (*figures 12(a)* and *(c)*) and increase in the outer layer. $\overline{v'^2}$ behaves differently in that it increases over most of the boundary-layer thickness in streamwise direction. *Figure 12(c)* shows that downstream of mean separation, $\overline{u'v'}$ changes sign in the swirling flow of the separation bubble. Positive values of $\overline{u'v'}$, combined with a positive value of the mean shear $\partial\overline{u}/\partial y$, lead to a negative production of turbulent kinetic energy (see *figure 13*).

Following the warning of Rotta [29] that the additional production terms

$$\left(\overline{u'^2} - \overline{v'^2}\right)\frac{\partial\overline{u}}{\partial y} \quad \text{and} \quad \overline{u'^2}\,\frac{\partial\overline{v}}{\partial x}$$

(see above) might play a role near separation, we have evaluated them where ever possible but found that they remained at least two orders of magnitude smaller than the production terms

$$-\overline{u'v'}\,\frac{\partial\overline{u}}{\partial y} \quad \text{and} \quad \overline{v'^2}\,\frac{\partial\overline{u}}{\partial y}.$$

Figures 13(a) and *(b)* show these two production terms non-dimensionalised by the displacement thickness δ_1 and $\overline{u}_{\delta(\overline{u'v'}=0)}$. For the two profiles closest to the fence, at $(x_f - x)/l_f = 0.38$ and 0.19, the production terms change sign in the near-wall region. Both profiles show mean flow in the negative x-direction with a negative mean velocity gradient near the wall. Therefore, the production term $\overline{v'^2}\,\partial\overline{u}/\partial y$ is negative in this region (see *figure 13*). For the production of turbulent kinetic energy, the situation is more complicated. For the profile at $(x_f - x)/l_f = 0.38$, $\overline{u'v'}$ is negative near the wall and in the upper region of the profile, but positive in a small

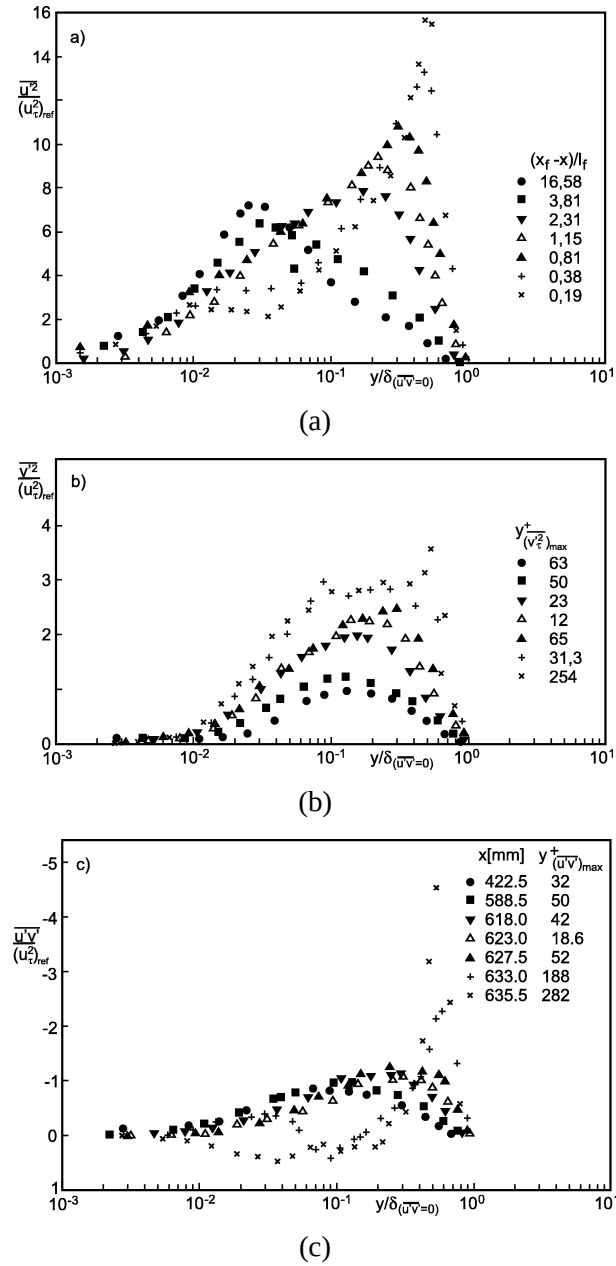

Figure 12. Streamwise development of the profiles of the Reynolds stresses in front of a fence: (a) $\overline{u'^2}/(u_\tau^2)_{\mathrm{ref}}$; (b) $\overline{v'^2}/(u_\tau^2)_{\mathrm{ref}}$; and (c) $\overline{u'v'}/(u_\tau^2)_{\mathrm{ref}}$.

region between $0.05 < y/\delta_{\overline{u'v'}=0} < 0.16$ (see *figure 12*). The velocity gradient $\partial\overline{u}/\partial y$ is positive, except for the immediate vicinity of the wall. Therefore, this profile shows two regions, where the production of turbulent kinetic energy is negative (see *figure 13*). Even closer to the fence, at $(x_f - x)/l_f = 0.19$, $\overline{u'v'}$ is positive from the wall up to $y/\delta_{\overline{u'v'}=0} \approx 0.25$. The production of turbulent kinetic energy is positive near the wall because of the negative velocity gradient. It is positive in the outer layer, where $\overline{u'v'}$ is negative and $\partial\overline{u}/\partial y$ is positive. In

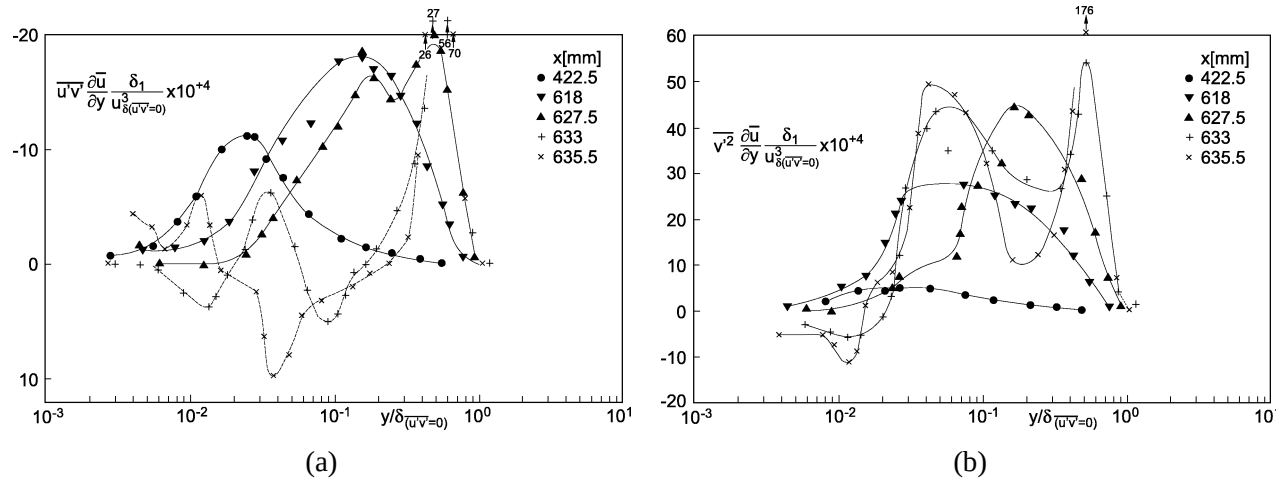

Figure 13. Profiles of the production terms in the transport equation for the turbulence kinetic energy (lines are for visual aid only).

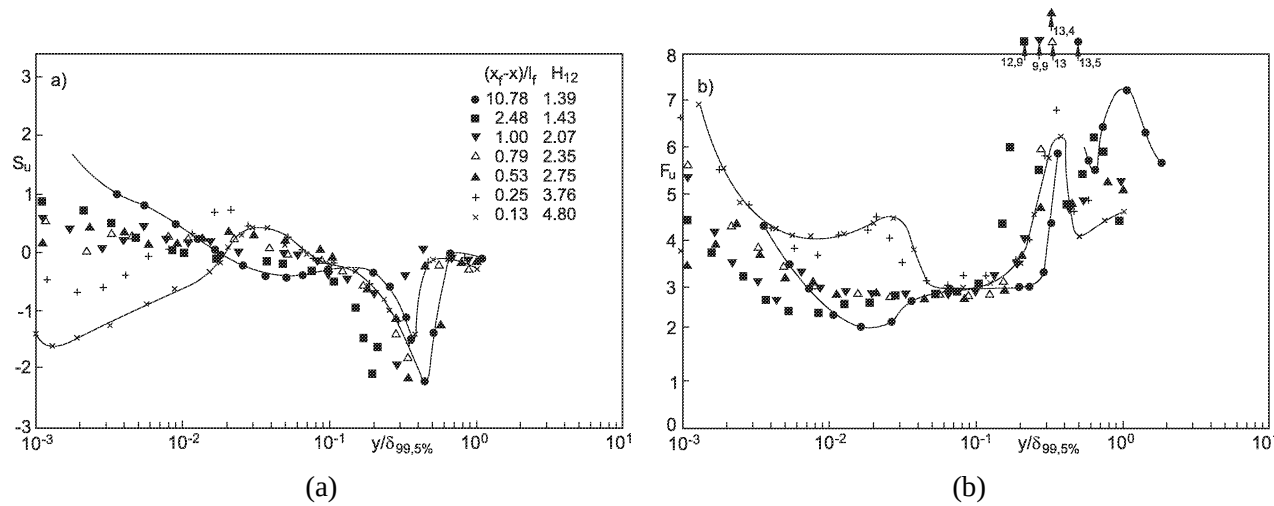

Figure 14. Profiles of higher moments of the streamwise velocity fluctuation: (a) skewness $\overline{u'^3}/(\overline{u'^2})^{3/2}$; (b) flatness $\overline{u'^4}/(\overline{u'^2})^2$.

between however, where $\overline{u'v'}$ and $\partial\overline{u}/\partial y$ are both positive, there is a region where the production of turbulent kinetic energy is negative (see *figure 13*).

Measurements so close to the wall could only be obtained by LDA and could not be made by Alving and Fernholz [24], for example. The high values of the production in the middle of the outer layer result both from high mean shear and high Reynolds shear-stress values.

The profiles of the skewness and flatness profiles across the boundary layer (*figures 14(a)* and *(b)*) show only a small effect of the pressure gradient in the outer 98% of the boundary layer. However, in the vicinity of the wall $S_{u'}$ reaches larger negative values in the reverse-flow region the closer the fence is approached. The flatness increases at about $y/\delta = 0.05$ by a factor of 1.5 and then reaches values very close to the wall which are much higher in the reverse-flow region than in the zero pressure-gradient boundary-layer (e.g. Fernholz and Finley [26]). The high values of $S_{u'}$ and $F_{u'}$ in the reverse-flow confirm the above result that free-stream fluid is transported more deeply into the near-wall region down the upstream side of the fence.

4. Conclusions

Experimental results for the mean and fluctuating values of the skin friction and the u- and v-components of the velocity reveal global features of the flow and give insight into the turbulence structure.

The measurements were taken with the fence fixed and the probe (the measuring volume of the LDA or the wall pulsed-wire) moved. Thus the length of the boundary layer between the leading edge of the plate and the fence and the ratio of boundary layer thickness measured without the fence to fence height $\delta_0/h = 0.82$ were kept constant.

The time mean separation line is 0.65 fence heights h upstream of the fence, whereas instantaneous reverse flow occurs up to four mean separation lengths l_f upstream of the fence. The separating streamline meets the upstream front of the fence at about $0.65h$. The maximum value of the reverse-flow factor χ_w is 95 %, indicating a strong reverse-flow region.

The higher moments of the fluctuating wall shear-stress and the velocity fluctuations indicate that the flow in the separation zone upstream of the fence is highly turbulent. Strong sweeping events occur in the reverse flow region near the fence and bring energised fluid down to the wall. A corner vortex at the foot of the fence exists only in the time mean (as opposed to a laminar separation), which can also be seen from flow visualisations.

Mean velocity profiles and Reynolds-stress profiles show in principle the behaviour typical of an adverse pressure gradient boundary-layer. However, the vertical velocity component and static pressure increase in the streamwise direction until very close to the fence and in the reverse-flow region all first-order boundary-layer assumptions cease to apply. The measurements indicate that classic boundary-layer theory can only be applied up to a distance not closer than $2l_f$ upstream of the fence. In this region, the standard definition of the boundary layer thickness becomes meaningless because of the slanted velocity profiles. However, the location where the Reynolds shear-stress $\overline{u'v'}$ approaches zero proved to be a useful new definition of the edge of the boundary layer.

A logarithmic velocity profile is only present for profiles with a reverse flow factor at the wall below $\chi_w = 1.0\%$. The inner-layer behaviour was dominated by a reduction of $\partial\overline{u}/\partial y$ and negative values of $\partial\overline{u}/\partial y$ occur in the closed reverse-flow region with positive values of $\overline{u'v'}$ leading to a partial cancellation of the turbulent energy production.

References

[1] Bradshaw P., Wong F.Y.F., The reattachment and relaxation of a turbulent shear layer, J. Fluid Mech. 52 (1972) 113–135.
[2] Castro I.P., Fackrell J.E., A note on two-dimensional fence flows, with emphasis on wall constraints, J. Ind. Aerodynamics 3 (1978) 1–20.
[3] Durst F., Rastogi A.K., Turbulent flow over two-dimensional fences, in: Bradbury L.J.S. (Ed.), 2nd Symposium on Turbulent Shear Flows, 1979, pp. 218–232.
[4] Dimaczek G., Kessler R., Martinuzzi R., Tropea C., The flow over two-dimensional, surface mounted obstacles at high Reynolds numbers, in: Proc. 7th Symposium on Turbulent Shear Flows, Stanford, CA, 1989, pp. 10.1.1–10.1.6.
[5] Schofield W.H., Logan E., Turbulent shear flow over surface mounted obstacles, J. Fluids Eng. 112 (1990) 376–385.
[6] Castro I.P., Epik E., Boundary layer development after a separated region, J. Fluid Mech. 374 (1998) 90–116.
[7] Siller H.A., Reduction of the recirculation length downstream of a fence by an oscillating cross-flow, Dissertation, Techn. Univ. Berlin, Mensch und Buch Verlag, Berlin, 1999.
[8] Tropea C.D., Gackstatter R., The flow over two-dimensional surface-mounted obstacles at low Reynolds numbers, J. Fluids Eng. 107 (1985) 489.
[9] Acharya S., Dutta S., Myrum T.A., Baker R.S., Turbulent flow past a surface-mounted two-dimensional rib, J. Fluids Eng. 116 (1994) 238–247.
[10] Bradshaw P., Galea P.V., Step-induced separation of a turbulent boundary layer in incompressible flow, J. Fluid Mech. 27 (1) (1967) 111–130.
[11] Head M.R., Rechenberg I., The Preston tube as a means of measuring skin friction, J. Fluid Mech. 14 (1962) 1–17.
[12] Fernholz H.-H., Three-dimensional disturbaces in a two-dimensional incompressible turbulent boundary layer, Reports and Memoranda 3368, ARC, London, 1964.

[13] Good M.C., Joubert P.N., The form drag of two-dimensional bluff-plates immersed in turbulent boundary layers, J. Fluid Mech. 31 (3) (1968) 547–582.
[14] Ranga Raju K.G., Loeser J., Plate E.J., Velocity profiles and fence drag for a turbulent boundary layer along smooth and rough flat plates, J. Fluid Mech. 76 (2) (1976) 383–399.
[15] Townsend A.A., The behaviour of a turbulent boundary layer near separation, J. Fluid Mech. 12 (1962) 536–554.
[16] Föttinger H., Mitteilungen der Vereinigung der Gross-Kesselbesitzer, 73 (1939) 151.
[17] Batchelor G.K., An Introduction to Fluid Dynamics, Cambridge University Press, 1967.
[18] Wieghardt K., Erhöhung des turbulenten Reibungswiderstands durch Oberflächenstörungen, Forschungshefte für Schiffstechnik 2 (1953) 65–81.
[19] Lighthill M.J., On boundary layers and upstream influence. I. A comparison between subsonic and supersonic flows, P. Roy. Soc. A 217 (1953) 344–357.
[20] Orellano A., Wengle H., Visualization of coherent structures in manipulated turbulent flow over a fence, in: IUTAM Symposium on 'Simulation and Identification of Organized Structures in Flows', Kluwer Academic Publishers, Dordrecht, Netherlands, 1999.
[21] Bradbury L.J.S., Castro I.P., A pulsed-wire technique for velocity measurements in highly turbulent flows, J. Fluid Mech. 49 (1971) 657–691.
[22] Castro I.P., Pulsed-wire anemometry, Exp. Therm. Fluid Sci. 5 (1992) 770–780.
[23] Dengel P., Fernholz H.-H., An experimental investigation of an incompressible turbulent boundary layer in the vincinity of separation, J. Fluid Mech. 212 (1990) 615–636.
[24] Alving A.E., Fernholz H.-H., Turbulence measurements around a mild separation bubble and downstream of reattachment, J. Fluid Mech. 322 (1996) 297–328.
[25] Fernholz H.-H., Near–wall phenomena in turbulent separated flows, Acta Mech. 4 (1994) 57–67.
[26] Fernholz H.-H., Finley P.J., The incompressible zero-pressure-gradient turbulent boundary layer: An assessment of the data, Prog. Aerospace. Sci. 32 (1996) 245–311.
[27] Spalart P.R., Direct simulation of a turbulent boundary layer up to $R_\theta = 1410$, J. Fluid Mech. 187 (1988) 61–98.
[28] Khanna S., Structure of the atmospheric boundary layer from large eddy simulation, PhD thesis, Pennsylvania State University, The Graduate School, Department of Mechanical Engineering, 1995.
[29] Rotta J.C., Turbulent boundary layers in incompressible flow, Prog. Aeronaut. Sci. 2 (1962) 5–219.